CORA Cork Open Research Archive
Cartlann Taighde Oscailte Chorcaí

Title	Binary mixtures of flufenamic acid and its chloro, difluoromethyl and fluoromethyl analogues; incorporation and distribution in flufenamic acid crystals
Authors	Bourke, Timothy;Chiarella, Renato A.;Moynihan, Humphrey A.
Publication date	2026-08-10
Original Citation	Bourke, T, Chiarella, R A & Moynihan, H A 2026, 'Binary mixtures of flufenamic acid and its chloro, difluoromethyl and fluoromethyl analogues; incorporation and distribution in flufenamic acid crystals', CrystEngComm, vol. 28, no. 31, pp. 4516-4527. https://doi.org/10.1039/d6ce00346j
Type of publication	Article (peer-reviewed)
Link to publisher's version	https://www.scopus.com/pages/publications/105043794282 - 10.1039/d6ce00346j
Rights	© 2026, The Author(s). Published by the Royal Society of Chemistry. This article is licensed under a Creative Commons Attribution 4.0 Unported Licence. You can use material from this article in other publications without requesting further permissions from the RSC, provided that the correct acknowledgement is given. - https://creativecommons.org/licenses/by/4.0/
Download date	2026-11-01 12:31:01
Item downloaded from	https://hdl.handle.net/10468/19092

UCC
University College Cork, Ireland
Coláiste na hOllscoile Corcaigh

CrystEngComm

ROYAL SOCIETY OF CHEMISTRY

PAPER

Published on 06 July 2026
Licensed under CC-BY 4.0

Check for updates

Cite this: DOI: 10.1039/d6ce00346j

Binary mixtures of flufenamic acid and its chloro, difluoromethyl and fluoromethyl analogues; incorporation and distribution in flufenamic acid crystals

Timothy Bourke,[a] Renato A. Chiarella [b] and Humphrey A. Moynihan *[a]

Impurities are a common feature of pharmaceutical process chemistry. For example, fluorine-containing drug substances are often found to have the corresponding desfluoro compounds as impurities which are difficult to remove by crystallization. Analogues of flufenamic acid in which the trifluoromethyl group was replaced by difluoromethyl, fluoromethyl or chloro groups were synthesized and examined as examples of such impurities. Investigation of the extent of incorporation and behaviour by PXRD and DSC were consistent with crystal lattice level substitution of flufenamic acid molecules with analogous impurities. Use of methanol or acetonitrile as crystallization solvent resulted in efficient incorporation of the impurities into flufenamic acid crystals. Examination of the distribution of the impurities within flufenamic acid crystals by partial dissolution methods showed that impurity inclusion was occurring throughout the crystal growth process. In each of the impurities studied, the trifluoromethyl group of flufenamic acid was replaced by a group with similar electronic and steric properties. Consideration of the crystal structure of the flufenamic acid polymorph obtained, *i.e.*, form III, suggested that replacement of flufenamic acid molecules by those impurities could be accommodated within the flufenamic acid form III crystal lattice.

Received 28th April 2026,
Accepted 27th June 2026

DOI: 10.1039/d6ce00346j

rsc.li/crystengcomm

Introduction

Impurities are a common occurrence in the production of pharmaceutical drug substances.[1,2] For drug substances and intermediate products containing fluorine or other halogens, dehalogenated and related analogues often occur as impurities, and these are often difficult to remove by crystallization.[3,4] Strong incorporation of the impurities in the crystallizing entities may be occurring in such cases, which may be confirmed by investigation of the phase behaviour and nature of incorporation of the drug substance/impurity binary mixtures.[5,6]

Flufenamic acid (**FFA**) is a member of the fenamic acid series of non-steroidal anti-inflammatory drugs.[7] It exemplifies many materials issues displayed by drug substances, such as extensive crystal polymorphism.[8,9] A trifluoromethyl (CF_3) group is a notable feature of the structure of **FFA**, hence the corresponding difluoromethyl (CF_2H) and fluoromethyl (CFH_2) compounds (Fig. 1; **HF_2FA** and **H_2FFA**) would be close structural analogues of **FFA**. The analogue in which the trifluoromethyl group is replaced by a chloro group (Fig. 1; **ClFA**) would also be similar on steric and electronic grounds, *i.e.*, both groups possess similar van der Waals radii (2.15 Å *vs.* 1.80 Å respectively)[10] and electronegativities (3.35 eV *vs.* 3.03 eV respectively).[11] The relative sizes of the CF_3, CF_2H and CFH_2 groups can be compared through their Bondi volumes, a measure of molecular volume that accounts for both the van der Waals radii of atoms and the distances of the covalent bonds between them.[12,13] The Bondi volumes for the CHF_2 and CH_2F groups are 18.8 and 16.0 $cm^3\ mol^{-1}$ respectively, smaller than the CF_3 volume of 21.3 $cm^3\ mol^{-1}$, although

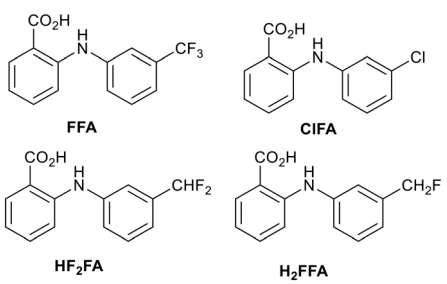


Fig. 1 Molecular structures of flufenamic acid (**FFA**) and *N*-(3-chlorophenyl)anthranilic acid (**ClFA**), *N*-(3-difluoromethyl)anthranilic acid (**HF_2FA**), *N*-(3-fluoromethyl)anthranilic acid (**H_2FFA**).

[a] *Analytical and Biological Chemistry Research Facility, School of Chemistry, Synthesis and Solid State Pharmaceutical Centre, University College Cork, College Road, Cork Y12 K8AF, Ireland. E-mail: h.moynihan@ucc.ie*
[b] *Pharmaceutical Development, Alkermes Inc., 900 Winter Street, Waltham, MA 02451, USA*

larger than the chloro group, which has a Bondi volume of 12.0 cm^3 mol^{-1}.[14] **ClFA** is known to have anti-inflammatory activity[15] and three crystal forms of **ClFA** have been reported, all in the triclinic $P\bar{1}$ space group.[16,17] **H_2FFA** has been reported as a treatment of progressive multifocal leukoencephalopathy.[18] The compound series **FFA**, **ClFA**, **HF_2FA** and **H_2FFA** provides a good basis for investigation of the inclusion of closely related impurities into **FFA** material. This work examines the inclusion of **ClFA**, **HF_2FA** and **H_2FFA** in crystals of **FFA**, in terms of overall inclusion, effect on phase behaviour as observed by PXRD and DSC, and in terms for distribution throughout the **FFA** crystals using partial dissolution and analysis methods developed previously.[19–21] In this way, the inclusion behaviour of these related substances can be thoroughly mapped out. Such information would be valuable for troubleshooting poorly performing crystallizations and designing effective process purifications.

Experimental

Synthesis of FFA analogues

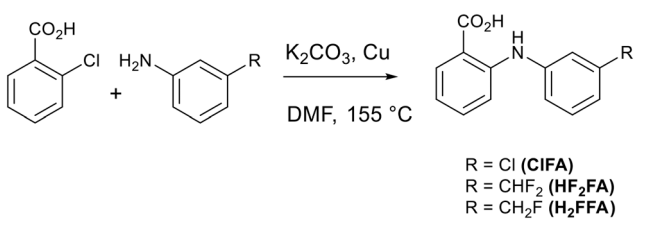
Starting materials, reagents and other materials were obtained from Sigma Aldrich. The **FFA** analogues **ClFA**, **HF_2FA** and **H_2FFA** were synthesised using a method reported by Pellón *et al.*[22] (Scheme 1).

2-Chlorobenzoic acid (1.25 g, 8 mmol) was added to a 100 mL flask with potassium carbonate (0.55 g, 4 mmol) and metallic copper (40 mg, 0.63 mmol) and the flask flushed with N_2 gas. The desired substituted aniline (16 mmol) and anhydrous *N*,*N*-dimethylformamide (5 mL) were added through a septum. The reaction was heated to 155 °C for 4 hours. The reaction mixture was cooled, then slowly added to *ca.* 6 M aqueous hydrochloric acid (20 mL with washings) and allowed to stand for several hours. The resulting precipitate was isolated *via* vacuum filtration and rinsed with dilute aq. hydrochloric acid. The solid was redissolved in ethyl acetate, activated charcoal (*ca.* 1 g) added, and the mixture filtered through Celite®. The filtrate was washed with hot water (3 × 30 mL) and dried over anhydrous magnesium sulfate. The solvent was removed by rotary evaporation to isolate the crude product which was recrystallized from toluene.

N-(3-Chlorophenyl)anthranilic acid (**ClFA**) was obtained as a sand-coloured powder (71%); m.p. 169.5–169.9 °C (lit.[23] 171–173 °C); IR ν_{max} (cm^{-1}) 3332 (amine N–H stretch), 2922 (acid O–H stretch), 1669 (acid C═O stretch), 1587 (ar. C–C stretch), 1518 (amine N–H bend), 1449 (acid O–H bend), 1258, 1238, 1155 (C–N stretches), 1150–1000 (ar. C–Cl stretches) 925, 890, 767, 744, 680 (ar. C–H bends) [SI Fig. S1]; ^{1}H NMR 300 MHz, δ_H (MeOD) 6.80–6.85 (1H, t, *J* 7.6 Hz, C(10)*H*), 7.00–7.03 (1H, dd, *J* 8.0, 1.0 Hz, C(4)*H*), 7.12–7.14 (1H, dd, *J* 8.0, 1.0 Hz, C(2)*H*), 7.21 (1H, s, C(5)*H*), 7.26–7.32 (2H, m, C(8)*H* and C(9)*H*), 7.36–7.41 (1H, t, *J* 8.0 Hz, C(3)*H*), 7.98–8.01 (1H, d, *J* 7.6 Hz, C(11)*H*), O*H* and N*H* signals not observed [SI Fig. S2]; ^{13}C NMR 100.6 MHz, δ_C (MeOD) 114.08 (*C*(12)), 114.89 (*C*(8)H), 118.62, 118.82 (*C*(4)H and *C*(10)H), 119.82 (*C*(5)H), 122.15 (*C*(2)H), 130.96 (*C*(3)H), 131.91 (*C*(11)H), 133.82 (*C*(1)Cl), 134.14 (*C*(9)H), 142.65 (*C*(6)), 145.69 (*C*(7)), 169.70 (*C*(13)) [SI Fig. S3 and S4]; *m*/*z* (ESI^+): 248.2 $[M + H]^+$, *m*/*z* (ESI^-): 246.3 $[M - H]^-$, HRMS: $C_{13}H_{10}ClNO_2$, predicted *m*/*z* 248.047283, measured *m*/*z* 248.04743 $[M + H]^+$, i-FIT confidence (%) 100.000 000.

N-(3-Difluoromethyl)anthranilic acid (**HF_2FA**) sand-coloured or brown needles (73%); m.p. 141.4–142.5 °C; IR ν_{max} (cm^{-1}) 3336 (amine N–H stretch), 2928 (acid O–H stretch), 2473, 2231, 2064 (alkyl C–H stretches), 1665 (acid C═O stretch), 1560 (ar. C–C stretch), 1495 (amine N–H bend), 1447 (acid O–H bend), 1373 (C–F stretch), 1257, 1164 (C–N stretches), 899, 762, 741, 690, 649 (ar. C–H bends) [SI Fig. S5]; ^{1}H NMR 300 MHz, δ_H (MeOD) 6.53–6.90 (1H, t, *J* 56.3 Hz, C(1)*H*F_2), 6.76–6.82 (1H, ddd, *J* 7.5, 7.5, 1.2 Hz, C(11)*H*), 7.18–7.21 (1H, dd, *J* 7.5, 1.2 Hz, C(9)*H*), 7.25–7.28 (1H, dd, *J* 8.5, 1.0 Hz, C(5)*H*), 7.31–7.45 (4H, m, C(3)*H* and C(4)*H* and C(6)*H* and C(10)*H*), 7.98–8.01 (1H, dd, *J* 7.5, 1.2 Hz, C(12)*H*), O*H* and N*H* signals not observed [SI Fig. S6]; ^{13}C NMR 75.5 MHz, δ_C (MeOD) 112.98–119.27 (t, *J* 237.2 Hz, *C*(1)HF_2), 114.42 (*C*(13)), 115.20 (*C*(9)H), 119.02–119.27 (*C*(11)H and t, *J* 6.1 Hz, *C*(6)H), 120.80–120.96 (t, *J* 6.1 Hz, *C*(3)H), 124.29–124.65 (t, *J* 2.0 Hz, *C*(5)H), 130.96 (*C*(4)H), 133.36 (*C*(12)H), 135.13 (*C*(10)H), 137.13–137.72 (t, *J* 22.3 Hz, *C*(2)), 143.03 (*C*(7)), 148.31 (*C*(8)), 171.71 (*C*(14)) [SI Fig. S7 and S8]; *m*/*z* (ESI^+): 264.3 $[M + H]^+$, *m*/*z* (ESI^-): 262.3 $[M - H]^-$, HRMS: $C_{14}H_{11}F_2NO_2$, predicted *m*/*z* 264.083061, measured *m*/*z* 264.08265 $[M + H]^+$, i-FIT confidence (%) 100.000 000.

N-(3-Fluoromethyl)anthranilic acid (**H_2FFA**) yellow powder (69%); m.p. 154.6–157.9 °C; IR ν_{max} (cm^{-1}) 3337 (amine N–H stretch), 2965 (acid O–H stretch), 2640, 2566, 2474 (alkyl C–H stretches), 1670 (acid C═O stretch), 1580 (ar. C–C stretch), 1521 (amine N–H bend), 1450 (acid O–H bend), (C–F stretch), 1244, 1162 (C–F and C–N stretches, overlapping), 965, 892, 742, 693, 656 (ar. C–H bends) [SI Fig. S12]; ^{1}H NMR 300 MHz, δ_H (MeOD) 5.25–5.41 (2H, d, *J* 47.8 Hz, C(1)*H*$_2$F), 6.72–6.78 (1H, ddd, *J* 7.5, 7.5, 1.3 Hz, C(11)*H*), 7.05–7.08 (1H, dd, *J* 7.5, 1.3 Hz, C(9)*H*), 7.19–7.26 (3H, m, C(3)*H* and C(5)*H* and C(6)*H*), 7.30–7.37 (2H, m, C(4)*H* and C(10)*H*), 7.97–8.00 (1H, dd, *J* 7.5, 1.3 Hz, C(12)*H*), O*H* and N*H* signals not observed [SI Fig. S13 and S14]; ^{13}C NMR 75.5 MHz, δ_C (MeOD) 84.14–86.34 (d, *J* 165.3 Hz, *C*(1)H_2F), 113.95 (*C*(13)), 115.04 (*C*(9)H), 118.53 (*C*(11)H), 121.43–121.51 (d, *J* 6.1 Hz, *C*(6)H), 120.70–120.74 (d, *J* 2.8 Hz, *C*(5)H), 123.05–123.13 (d, *J* 6.1 Hz, *C*(3)H), 130.67–130.68 (d, *J* 1.1 Hz, *C*(4)H), 133.29 (*C*(12)H), 135.08 (*C*(10)H), 139.31–139.54 (d, *J* 17.1 Hz, *C*(2)), 142.67 (*C*(7)), 148.80 (*C*(8)),



Scheme 1 Syntheses of **ClFA**, **HF_2FA** and **H_2FFA**.

 This journal is © The Royal Society of Chemistry 2026

171.81 (*C*(14)) [SI Fig. S15 and S16]; *m*/*z* (ESI$^+$): 246.3 $[M + H]^+$, *m*/*z* (ESI$^-$): 244.3 $[M - H]^-$, HRMS: $C_{14}H_{12}FNO_2$, predicted *m*/*z* 246.092 483, measured *m*/*z* 246.09143 $[M + H]^+$, i-FIT confidence (%) 100.000 000.

HPLC. HPLC data was obtained from an Agilent 1290 Infinity II LC System interfaced to a Dell OptiPlex 5040. Instrument control and data processing was performed using Agilent OpenLab ChemStation software. A Zorbax Eclipse Plus UHPLC column was used with a mobile phase consisting of 50 : 50 ratio of acetonitrile and a 0.1% v/v aqueous solution of trifluoroacetic acid, the detector was set at 280 nm, the flow rate at 0.5 mL min^{-1}, the injection volume 2 μL, and the column temperature set to 30 °C. Calibration curves and accompanying statistics for each of **FFA**, **ClFA**, **HF_2FA** and **H_2FFA** are shown in the SI in Fig. S20–S23 and Tables S1–S8. Examples of HPLC traces of solutions of **FFA** containing each of **ClFA**, **HF_2FA** and **H_2FFA** are shown in the SI in Fig. S24–S26.

PXRD. PXRD was performed at ambient temperature using a STOE STADI-MP diffractometer operating in transmission mode with a linear PSD detector with an anode current of 40 mA, an accelerating voltage of 40 kV and Cu Kα_1 radiation (λ = 1.5406 Å) scanning in steps of 1.0° for 30 seconds per step from 5 to 35° in 2θ. Samples were held between clear acetate foils. Examples of experimental PXRDs of **FFA** and comparison with literature data are shown in SI Fig. S27. There is extensive literature on the polymorphism of **FFA.**[24–31] Form III is the thermodynamically stable form at room temperature and was selected for use in this study. **ClFA** is, so far, the only one of the three FFA analogues that is known to be polymorphic.[17] The material produced in this study was found to be the form I polymorph (SI Fig. S28).

Solubility measurements. Solubilities of **FFA** form III were measured in a range of solvents (Table 1). The saturation points were determined by the excess solid method.[32] The sample flask was immersed in a DrySyn® heating block on an IKA RCT Basic® hot plate set to 25 °C. The suspended solid was agitated in the solvent using a magnetic stirrer bar for up to 3 hours, after which 1 mL of saturated solution was removed through a 0.20 μm membrane syringe filter (Agilent 13 mm, PTFE Econofltr®) and added to a vial with washings. The process was repeated to give at least three samples per experiment, allowing for at least 15 minutes between aliquot collections. The solvent in each sample was completely removed by evaporation under high vacuum and the mass of the dry sample was determined using a Mettler Todelo ML203 microbalance.

Solubility in MTBE was found to be too high for effective crystal growth. Ethyl acetate, ethanol, methanol, toluene and acetonitrile were all found to the be acceptable solvents for **FFA** crystallizations, however a series of initial crystallization experiments found that methanol and acetonitrile were the best solvents for effective crystallizations. The relatively low solubility of **FFA** in hexane meant that hexane was a good solvent for carrying out controlled dissolutions and for use as an antisolvent.

Using the same methods, it was also possible to determine solubility data for **ClFA** in a narrower range of solvents (Table 2). It was not possible to obtain sufficient quantities of **HF_2FA** or **H_2FFA** to determine the solubilities of those compounds by these methods.

FFA crystallization from methanol. **FFA** was dissolved in sufficient MeOH to give subsaturated solutions which were filtered through a syringe filter into a vial or conical flask. The vials or flasks were then covered with perforated lids and allowed to rest until crystals were obtained but were not allowed to evaporate to dryness. The crystals were rinsed with cold hexane and dried under vacuum.

FFA crystallization from methanol with hexane vapour diffusion. **FFA** was dissolved in enough MeOH to give a subsaturated solution which was filtered through a syringe filter into a large vial. The vial was placed in a beaker containing a volume of hexane twice that of the MeOH solution and an airtight seal was fitted over the mouth of the beaker, which was allowed to rest until crystals were observed to form. The crystals were removed from the solution, rinsed with cold hexane, and dried under vacuum.

FFA crystallization from acetonitrile. To a volume of acetonitrile was added a mass of **FFA** solid 1.5 times its solubility at 25 °C. The suspension was heated in an oil bath to 80 °C until all material was fully dissolved, after which the solution was allowed to cool to room temperature. The excess solution was removed using a Pasteur pipette and the crystals rinsed with cold hexane and fully dried under high vacuum.

FFA crystallization from dichloromethane/hexane by rotary evaporation. **FFA** solid was dissolved in dichloromethane (*ca.* 100 mL g^{-1} **FFA**) in a 500 mL round-bottomed flask to give an undersaturated solution and twice the volume of hexane was added. The solvent mixture was evaporated by rotary evaporation (Buchi R-210 Rotavapor) at room temperature to give a slurry of **FFA** in hexane, which was isolated by filtration, washed with cold hexane and dried under vacuum.

Crystallization of FFA containing analogues ClFA, HF_2FA or H_2FFA. Quantities of **FFA** and of the required analogue (**ClFA**, **HF_2FA** or **H_2FFA**) were weighted out to give the required molar ratio of **FFA** to analogue. The quantities of the **FFA** and the analogue were separately dissolved in ethanol and the solutions mixed, filtered through a filter suitable for HPLC sample preparation, evaporated and thoroughly dried under vacuum, and the resulting solid subjected to the desired crystallization method as outlined

Table 1 Solubility of form III FFA in selected solvents at 25 °C

Solvent	Hexane	MeCN	Toluene	MeOH	EtOH	EtOAc	MTBE
Solubility/g L^{-1}	2.40	57.99	66.40	180.52	377.83	377.83	758.95

Table 2 Solubility of **ClFA** in selected solvents at 25 °C

Solvent	Hexane	MeCN	MeOH	EtOH
Solubility/mol L^{-1}	0.005	0.042	0.155	0.222

above. The ratio of **FFA** to additive was determined by HPLC. Slow evaporation from methanol was used to successfully produce large prismatic crystals of **FFA** containing low levels of **ClFA** or **HF_2FA**. Inclusion of **H_2FFA** produced crystals smaller than those of pure **FFA**, often having very fine acicular habits. Slow cooling from acetonitrile gave large acicular crystals with 2 to 5% analogue. Vapour diffusion produced large prismatic crystals containing low levels of **ClFA** and **HF_2FA**. Crystallization from dichloromethane/hexane produced very small acicular crystals. While crystals of **FFA** were of a pale yellow colour [SI Fig. S29], inclusion of the analogues produced a darker colouration, especially for higher levels of **HF_2FA** and **H_2FFA**.

Crystallization from methanol or from methanol with hexane vapour diffusion gave reasonably well-formed FFA crystals suitable for incorporation and/or partial dissolution studies. Crystallization from acetonitrile could give adequately prismatic crystals but gave very acicular crystals, suitable for segmentation analysis, upon slow cooling. Crystallization from dichloromethane/hexane by rotary evaporation was effective for producing crystals for DSC studies.

DSC. DSC analysis was carried out on a TA Q1000 Calorimeter with an RCS 40 cooling system. Ramping was carried out from approximately 15 °C to 180 °C in aluminium pans at a heating rate appropriate to the experiment. Masses of samples fell between 2–5 mg.

Partial dissolutions

Based on the relative solubilities shown in Table 1 above, hexane was chosen as the best solvent to allow controlled partial dissolutions for **FFA** samples. The sample crystals were suspended in hexane in a glass vial. The volume of hexane was selected to dissolve approximately 15% of the sample, based on the solubility of the **FFA** in hexane at 19 °C (0.99 mg mL^{-1}). The suspensions were agitated at a rate of 300 rpm for 90 minutes using Fisherbrand ZX3 Vortexer or a VWR incubating orbital mini shaker, after which the crystals were washed with cold hexane and dried. The mass and size of the crystals were measured, and the process repeated for the desired number of dissolution stages. Initial studies found addition of a surfactant to be unnecessary.

Smaller crystals were imaged using a Nikon Eclipse 50i polarising microscope with a Nikon Digital Sight DS-Fi1 digital camera. NIS-Elements software version BR 3.1 was used to analyse the images. Crystal perimeters were defined by thresholding for measurement of the resulting surface area which was doubled to give a measure of crystal surface areas. Lengths were measured between the longest observed crystal dimensions. For larger crystals, an Honor 7× dual 16 MP camera, mounted on a stable retort stand, with high dynamic range and phase detection auto focus was used. The crystals were photographed on a glass slide set atop a matte black surface, including a scale, in a manner that minimised glare and maximised contrast between the crystals and the background. The images were analysed using ImageJ image analysis software. The image was converted to 8-bit greyscale, and the "find edges" and "binary analysis" features used to outline the particles. Any gaps in the outline were filled manually using the "paint" tool. The areas within the outlines can be measured using the tracing and measuring tools, and the measured areas presented as mm^2 values, which were doubled to give the surface area of the measured face. Care was taken to optimise the quality of the images captured in terms of lighting, positioning, and the use of a camera mount, to minimise blur and glare. Samples were weighed using a Mettler Toledo MT5 microbalance. For samples containing both **FFA** and analogues **ClFA**, **HF_2FA** or **H_2FFA**, the levels of **FFA** and analogue in the solution collected after each dissolution stage was determined by HPLC. SI Fig. S30 gives an example of the results of a series of partial dissolution stages on the size of a sample of 20 **FFA** crystals.

Results and discussion

The **FFA** analogues **ClFA, HF_2FA** and **H_2FFA** were synthesised by coupling of 2-chlorobenzoic acid with the corresponding substituted aniline based on a method reported by Pellón *et al.*[22] and a HPLC system was developed allowing separation and quantification of mixtures of **FFA** and **ClFA**, **HF_2FA** or **H_2FFA**. As noted in the Experimental section, form III is the thermodynamically stable form of **FFA** at room temperature (*ca.* 20 °C), while form I is kinetically stable at that temperature, transforming into Form III in the solid state over a period of days. Form I becomes the thermodynamically stable form at temperatures above approximately 42 °C. Form III was selected for use in this study. Of the **FFA** analogues, **ClFA** is the only so far that is known to have polymorphic forms.[17] The **ClFA** material produced was determined to crystallize in the form I polymorph (SI Fig. S28). The **FFA** molecules in **FFA** form III[27] and the **ClFA** molecules in **ClFA** form I[17] both possess an *anti*-conformation between the carboxylated phenyl ring and the trifluoromethylated or chlorinated phenyl ring, *i.e.*, those groups are oriented in opposing directions, whereas in **FFA** form I, for example, they are oriented in approximately the same direction. However, there are differences in the packing arrangements. **ClFA** form I crystallizes in the triclinic $P\bar{1}$ space group,[17] while **FFA** form III is monoclinic $C2/c$ and **FFA** form I monoclinic $P2_1/c$.[27]

Crystals of pure **FFA** and of **FFA** containing the analogues **ClFA**, **HF_2FA** or **H_2FFA** were grown from solvents selected on the basis of measured solubilities and initial crystallization experiments. The solvents selected were methanol, acetonitrile, dichloromethane and hexane, the last of these being used to reduce or control solubility. Slow evaporation

 This journal is © The Royal Society of Chemistry 2026

from methanol, or from methanol using vapour hexane diffusion, was most often found to provide prismatic **FFA** crystals suitable for dissolution studies. Use of acetonitrile as solvent could give adequately prismatic crystals but gave very acicular crystals upon slow cooling. Crystallization from dichloromethane/hexane solutions using selective removal of dichloromethane by rotary evaporation was effective for providing larger amounts of **FFA** crystalline material for investigation of phase behaviour.

The extent of incorporation of all three analogues into crystals of **FFA** were examined in a range of *ca.* 0 to 6% (molar ratio) added analogue, as such a range would cover the typical extents of impurities observed in API manufacturing processes. As **ClFA** was obtainable in greater quantities, the level of inclusion of that analogue was also examined in a wider range of levels. Parameters examined included the extent of analogue level in the crystallized materials relative to levels of analogue added to solutions, and the selectivity value defined by Urwin *et al.*[2] Fig. 2–4 show plots of levels of incorporation of **ClFA** into **FFA** crystals grown, respectively, from methanol solutions containing 0 to 6% or 0 to 90% **ClFA**, and from acetonitrile containing 0 to 6% **ClFA**. All of these plots show direct proportionality of **ClFA** levels in solution with extent of incorporation into **FFA** crystals, with slopes for the three plots each being slightly greater than one. These imply that **ClFA** was quite reasonably incorporated into **FFA** form III crystals.

Urwin *et al.* have proposed a parameter, the selectivity (α_1), to determine the extent of impurity rejection during a crystallization.[2] The selectivity parameter is labelled α_1 here in order to distinguish it from the Kitamura and Nakai distribution coefficient, α_2, discussed below. (Both sets of authors designate their parameters as α.) The selectivity, α_1, can be given as follows (eqn (1)).

$$\alpha_1 = \frac{X_S^i X_L^A}{X_L^i X_S^A} \quad (1)$$

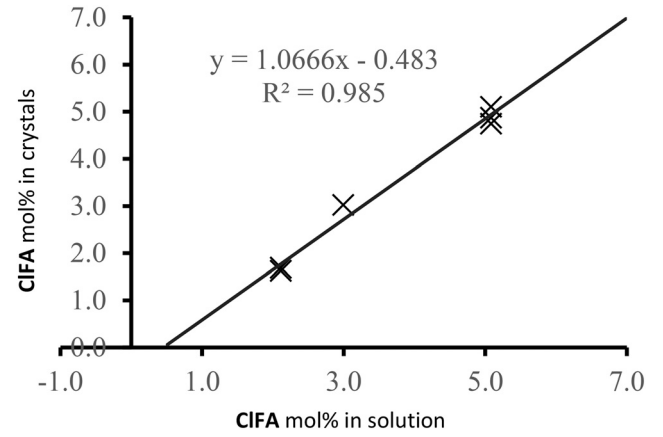


Fig. 2 Plot of incorporation of **ClFA** into **FFA** crystals *vs.* levels of **ClFA** added for crystal grown from MeOH containing 0 to 6% molar ratio **ClFA**.

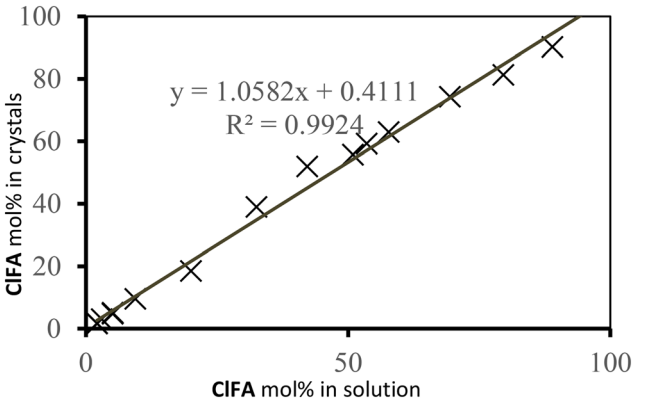


Fig. 3 Plot of incorporation of **ClFA** into **FFA** crystals *vs.* levels of **ClFA** added for crystal grown from MeOH containing 0 to 90% molar ratio **ClFA**.

In eqn (1), X stands for the mole fraction of either the impurity (i) or the drug substance (A), in either the recrystallized solid phase (S) or in the mother liquor phase (L), on a solvent-free basis. In this work, A refers to **FFA** and i refers to the analogue under consideration, *e.g.*, **ClFA** in this case. A crystallization which results in complete rejection of the impurity would give an α_1 value of zero. A value of one implies equal preference in the incorporation of impurity and API. Values of α_1 quite close to zero may imply impurities present due to surface deposition or absorption, which may be removable by washing or slurrying. Impurity incorporation due to, for example, solid solution formation, may be indicated by higher α_1 values. Table 3 shows α_1 values for crystallization of samples of **FFA** containing either 2% or 50% **ClFA** from acetonitrile. The initially obtained material was recrystallized a second time and the material obtained from that further recrystallized a third time, to ascertain whether there was any subsequent improvement on the selectivity, however the selectivity values remained relatively consistent over the series of recrystallizations. The

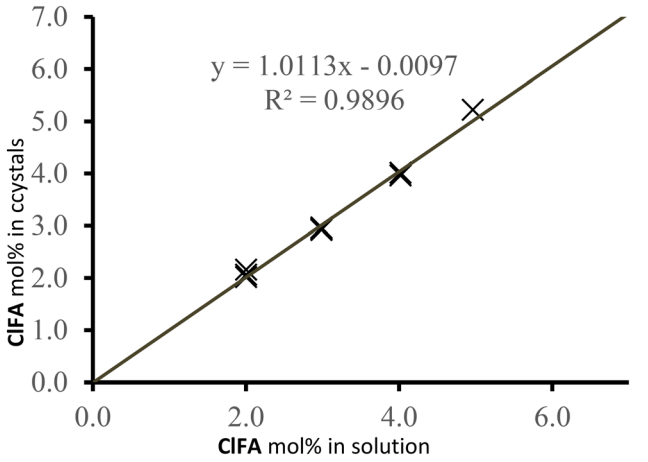


Fig. 4 Plot of incorporation of **ClFA** into **FFA** crystals *vs.* levels of **ClFA** added for crystal grown from MeCN containing 0 to 6% molar ratio **ClFA**.

Table 3 Selectivity (α_1) values for crystals of **FFA** produced by crystallization from acetonitrile of **FFA** crystals containing initial levels of analogue

Entry	Analogue	Initial level[a]	α_1	α_1 (1st repeat)[a]	α_1 (2nd repeat)[a]
1	**ClFA**	2 mol%	0.83	0.76	0.83
2	**ClFA**	50 mol%	4.51	5.34	5.12
3	**HF_2FA**	2 mol%	0.76	0.59	0.57
4	**H_2FFA**	2 mol%	0.61	0.62	0.61

[a] The crystallization process was repeated twice on each sample, using the solid obtained from the previous crystallization as the input material for the next.

selectivity values obtained for the **FFA** containing 2% **ClFA** was 0.83 for the first recrystallization. As described by Urwin *et al.*,[2] this selectivity value would imply that it would be difficult to free the **FFA** material of **ClFA** as an impurity using this crystallization method with this level of impurity in the feed material. The selectivity value for the 50% **FFA/ClFA** material was over 4.5 for each recrystallisation, suggesting a preference for inclusion of **ClFA** over **FFA** at this level, consistent with the phase behaviour observed at this composition range (discussed below). The selectivity value as determined for **FFA** as an impurity in **ClFA** crystals in this composition range is *ca.* 0.2, suggesting that it would be easier to develop a crystallization process to produce **ClFA** free of **FFA** impurity.

Fig. 5 and 6 show the extent of incorporation of **HF_2FA** and **H_2FFA**, respectively, into crystals of **FFA** grown from methanol relative to the extent of analogue in solution. Both are well incorporated, but to a lesser extent than the **ClFA** analogue. Table 2, entries 3 and 4, show the selectivity (α_1) values for **HF_2FA** and **H_2FFA**, respectively, over three successive crystallizations. These values imply that removing these analogues, if present as impurities in the input material at these levels, by such crystallizations would not be successful.

Fig. 7 shows the PXRD patterns of crystals containing both **FFA** and **ClFA**, as well as PXRDs of the pure components (**FFA** form III, **ClFA** form I). At levels of **ClFA** of 20% or lower, the patterns are consistent with that of **FFA** form III, while at **ClFA** levels of 30% or greater, they are consistent with the pattern for **ClFA** form I. Cases such as this, in which the crystal lattice of one compound gradually transforms into the lattice of another compound, through molecular substitutions and concomitant lattice adjustments, are known in the literature.[33]

As reported previously, DSC for **FFA** form III were found to display melting of form III followed by recrystallization and melting of form I, with the relative extents of the melting endotherms for forms I and III being altered by changing DSC heating rates.[21] Low heating rates were found to enhance the relative extent of the form I endotherm, while higher heating rates enhanced the relative extent of the form III endotherm. Presence of **ClFA** also appears to favour enhancement of the **FFA** form I endotherm, in particular at lower heating rates (SI Fig. S31). DSC data for **FFA/ClFA** mixtures were measured at a heating rate of 1 °C min^{-1}, to provide clear observation of the **FFA** form I melting endotherm. Fig. 8 shows DSC data for samples of **FFA/ClFA** obtained by crystallization from dichloromethane/hexane using the rotary evaporation method. These data are consistent with the inclusion data shown in Fig. 3 and also the PXRD data in Fig. 7, in they suggest that **FFA** form III and **ClFA** have a good degree of mutual inclusivity. SI Fig. S32–S34 show more detail on the emergence of the higher melting endotherm at **ClFA** levels above 20%, while SI Fig.

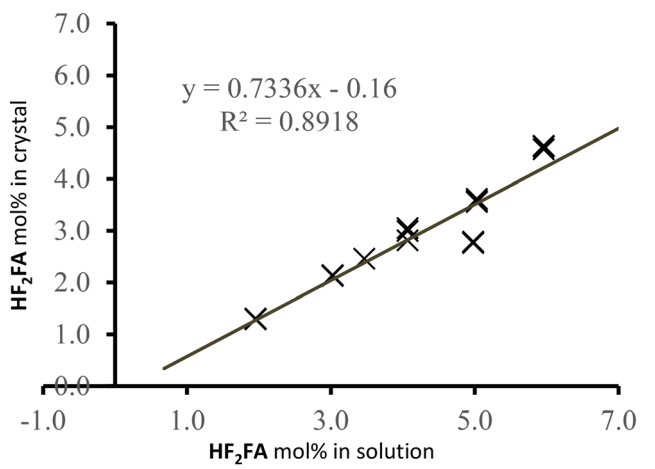


Fig. 5 Plot of incorporation of HF_2FA into FFA crystals *vs.* levels of HF_2FA added for crystal grown from MeOH.

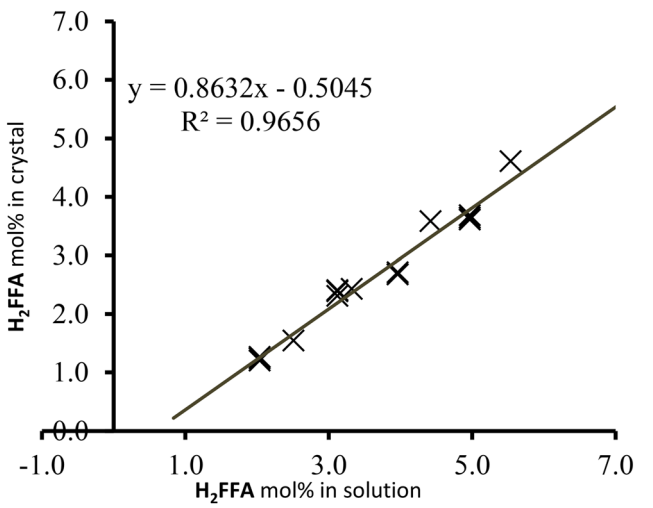


Fig. 6 Plot of incorporation of H_2FFA into FFA crystals *vs.* levels of H_2FFA added for crystal grown from MeOH.

This journal is © The Royal Society of Chemistry 2026

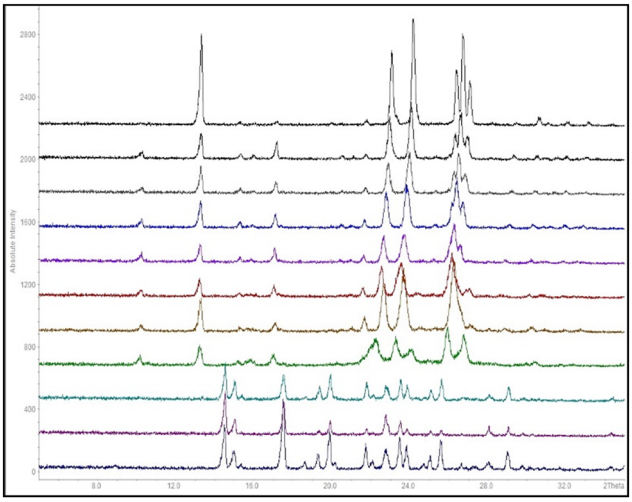


Fig. 7 PXRD patterns of crystals grown from methanol containing **FFA** and **ClFA** with **ClFA** levels of, from bottom to top, 0%, 10%, 20%, 30%, 40%, 50%, 60%, 70%, 80%, 90% and 100%.

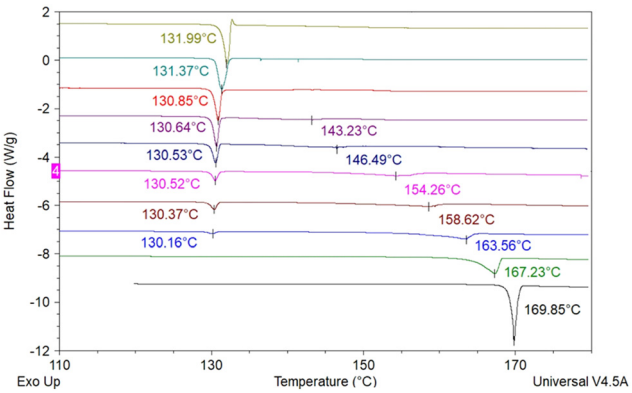


Fig. 8 DSC scans, recorded at a heating rate of 1 °C min^{-1}, of samples of **FFA/ClFA** crystallised from dichloromethane/hexane by rotary evaporation, of, top to bottom, **FFA** containing 10%, 20%, 30%, 40%, 50%, 60%, 70%, 80% and 90% **ClFA**, and (bottom) 100% **ClFA**.

S35 shows more detail on the melting endotherm at low **ClFA** levels. SI Fig. S33 shows the emergence of a higher melting endotherm at *ca.* 26% **ClFA**, while SI Fig. S34 shows this higher melting endotherm being well established at higher **ClFA** levels, corresponding to melting of essentially a **ClFA**-rich **ClFA/FFA** phase. SI Fig. S35 shows that at lower **ClFA** levels, only a single endotherm is observed, corresponding to melting of **FFA** form I containing levels of **ClFA**.

The incorporation data (Fig. 3), PXRD data (Fig. 7) and DSC data (Fig. 8) all indicate a mutual inclusivity of **FFA** or **ClFA** molecules in the solid state of the other component. This is consistent with the similar sizes and electronegativities of the CF_3 and Cl groups. The phase behaviour could be characterised as eutectic with solid solutions, albeit with some untypical features. DSC data for *ca.* 30% to 80% **ClFA**, *e.g.*, Fig. 8 and S34, are consistent with eutectic behaviour. At **ClFA** levels of *ca.* 20% or lower, eutectic and **FFA** melting are not visible as distinct endotherms (Fig. S32, S33 and S35). This may be because the solubility limit for the **FFA/ClFA** solid solution at low **ClFA** levels is close to the eutectic point. The PXRD data (Fig. 7) is supportive of inclusion of low levels of **ClFA** in an **FFA** form III lattice, and of moderate to low levels of **FFA** in a **ClFA** form I lattice, with transformation between lattices at *ca.* 25% **ClFA**.

As noted, both **FFA** and **ClFA** are polymorphic, with **FFA** form III and **ClFA** form I being the observed forms by PXRD in this work. In DSC, melting of **FFA** form III is observed followed by transition or recrystallization and melting of form I, with the relative extents of the melting endotherms depending on heating rates.[21] DSC of **ClFA**, showed a single endotherm, consistent with **ClFA** form I melting. The **FFA/ClFA** system must contain temperature-composition domains in which these various forms are stable or metastable, metastability being suggested by the effect of variations in DSC heating rate. The eutectic and solid solution type behaviours noticed would also be part of the full system, as well as the other known polymorphs of both compounds, and potentially other forms. Hence, **FFA/ClFA** would be a system of some complexity in its full phase behaviour.

Crystallization of quantities of **FFA** containing levels of **HF_2FA** or **H_2FFA** was found to enhance appearance of the **FFA** form III melting endotherm relative to that of form I, as observed in previous research on the analogue 2-(3-tolylamino) benzoic acid.[21] Hence, to allow clear observation of the **FFA** form III endotherm, DSC data was obtained as described in that work, *i.e.*, at a higher heating rate of 10 °C min^{-1} without sample grinding. DSC data on samples for **FFA** containing low levels of **HF_2FA** or **H_2FFA** are shown in Fig. S36 and S37. Evaluation of the full range of compositions was not possible for **HF_2FA** or **H_2FFA**. For both analogues, at the low incorporation levels studied, the behavior as indicated by DSC is largely similar to that of **FFA** form III, *i.e.*, that low levels of these analogues likely form solid solutions with **FFA** form III. Both **HF_2FA** and **H_2FFA** are more directly similar to **FFA** than **ClFA**, differing only in replacement of one or two fluorines of **FFA** with hydrogens. As noted in the Introduction, the Bondi volumes for the CHF_2 and CH_2F groups are 18.8 and 16.0 cm^3 mol^{-1} respectively, which are smaller than the CF_3 volume of 21.3 cm^3 mol^{-1} but larger than that of the chloro group (12.0 cm^3 mol^{-1}). Solid solution behaviour of crystallized **FFA** containing low levels of **F_2HFA** or **FH_2FA** would therefore be reasonable.

Partial dissolutions using hexane allowed samples of crystals of **FFA** to be subjected to a series of multiple dissolutions, with HPLC analysis of the solutions obtained from each dissolution step if required. The levels of crystal dissolution achieved in each stage were reasonably close to an approximate target level of 15% by mass, *e.g.*, one example of a series of four partial dissolutions of a sample of 49 **FFA** crystals at 21 °C dissolved 17%, 18%, 14% and 14% by mass in each respective step. The sizes of the crystals in the samples, as determined by image analysis over the multiple

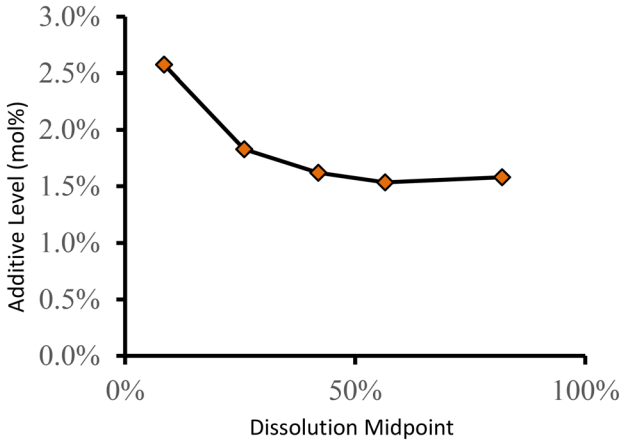


Fig. 9 Plot of **ClFA** level *vs.* dissolution midpoint of a sample of 49 crystals of **FFA** grown from solutions containing 2% molar ratio **ClFA**.

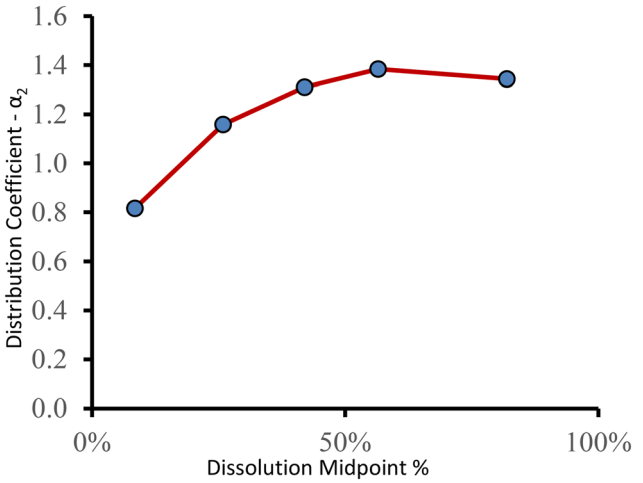


Fig. 10 Plot of α_2 value *vs.* dissolution midpoint of a sample of 49 crystals of **FFA** grown from solutions containing 2% molar ratio **ClFA**.

dissolution stages, could be presented as size distribution plots, as shown in previous published work.[19–21]

Partial dissolutions of **FFA** crystals grown from solutions containing 2% **ClFA**, with HPLC analysis of the solutions resulting from each dissolution, were carried out on samples of individual crystals, on samples of 10 crystals and on samples of 49 crystals. HPLC analysis of the solutions resulting from partial dissolutions (Fig. 9 and S38 and S39) consistently showed that **ClFA** had been incorporated at all stages of crystal growth. Incorporation levels were usually highest in the outer layers of the crystals, generally slightly higher than 2%, but were at levels slightly below 2% in the interior bulk of the crystals.

Another way of considering the partial dissolution data is to interpret it in terms of the distribution coefficient, α_2, (eqn (2)), proposed by Kitamura and Nakai.[34] The α_2 value gives a measure of the purification achieved during the crystallization. Higher α_2 values can arise as a consequence of higher mole fractions of the impurity in the liquid phase, *i.e.*, due to higher X_i^L values. Higher α_2 values can also arise as a consequence of higher mole fractions of the crystallizing compound, *e.g.*, the API, in the solid phase, as quantified by higher $(1 - X_i^S)$ values. Hence, higher α_2 values are characteristic of higher purity. Lower α_2 values can be a consequence of higher mole fractions of the impurity in the solid phase, *i.e.*, higher X_i^S values, or of higher mole fractions of the crystallizing compound in the liquid phase, *i.e.*, higher $(1 - X_i^L)$ values. Hence, lower α_2 values are indicative of lower purity. The selectivity parameter, α_1, of Urwin *et al.* and the distribution coefficient, α_2, of Kitamura and Nakai, are clearly related, *e.g.*, they are inverses of each other in a system of strictly one crystallizing component and one impurity component, and in principle either could be used. However, the selectivity parameter, α_1, was proposed to assist decision making in crystallization design while the distribution coefficient, α_2, was designed to assist determination of average composition, hence either may be preferable depending on the context.

Fig. 10 shows the α_2 values for the series of partial dissolutions shown in Fig. 9, determined using the HPLC data obtained after each dissolution step. The α_2 values show that the degree of discrimination of **FFA** over **ClFA** achieved by the crystallization process decreased as the crystals grew, except for a modest increase in the early stages of the process. Fig. S40 (SI) shows similar data for a sample of 14 **FFA** crystals, and for a large single crystal of **FFA**, grown from solutions containing 2% **ClFA**, showing the same trend in decreasing purification performance.

$$\alpha_2 = \frac{X_i^L\left(1 - X_i^S\right)}{X_i^S\left(1 - X_i^L\right)} \quad (2)$$

A similar pattern was found for crystals of **FFA** grown from solutions containing 2% **HF_2FA**. An example is shown in Fig. 11 (and further examples in SI Fig. S41) and, in terms of α_2 variation, in Fig. 12. Crystals of **FFA** from solutions containing 2% **H_2FFA** were smaller and more fragile than

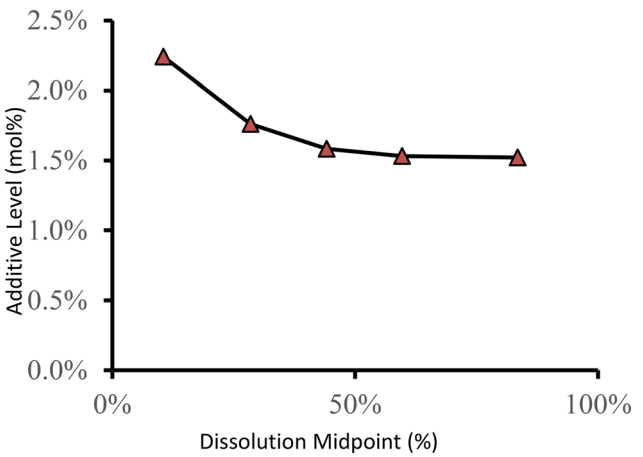


Fig. 11 Plot of **HF_2FA** level *vs.* dissolution midpoint of a sample of crystals of **FFA** grown from solutions containing 2% molar ratio **HF_2FA**.

This journal is © The Royal Society of Chemistry 2026

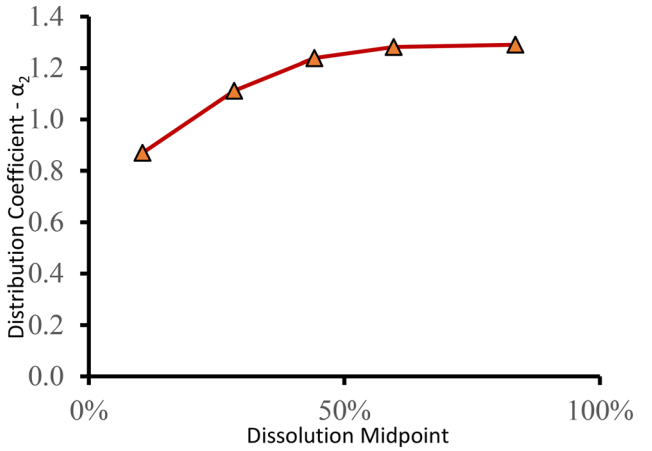


Fig. 12 Plot of α_2 value *vs.* dissolution midpoint of a sample of crystals of **FFA** grown from solution containing 2% molar ratio **HF_2FA**.

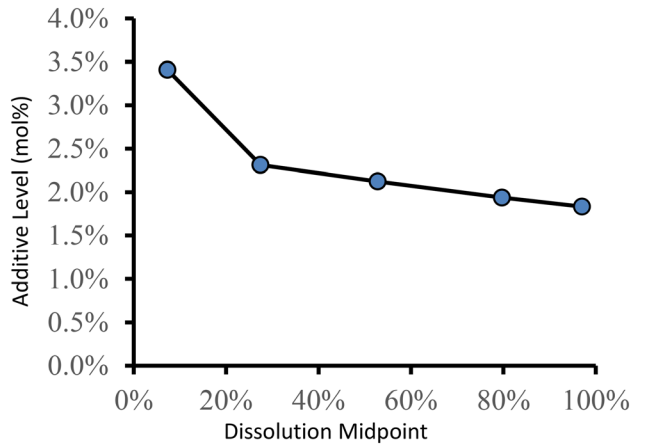


Fig. 13 Plot of **H_2FFA** level *vs.* dissolution midpoint of a sample of crystals of **FFA** grown from solutions containing 2% molar ratio **H_2FFA**.

those previously obtained. Nonetheless, partial dissolution experiments could be used to map the distribution of the **H_2FFA** impurity in terms of overall level (Fig. 13) or variation in α_2 value (Fig. 14).

Previous work had found that slow cooling of saturated solutions of **FFA** in acetonitrile could form clusters of extremely elongated needles growing outwards from a single nucleation point, and described a segmentation analysis approach to determining variations in levels of impurity incorporation during crystal growth.[21] Table 4 shows data on the levels of **ClFA**, **HF_2FA** and **H_2FFA** in such crystals, in which segment *a* is that closest to the nucleation point, segment *b* is the central segment and segment *c* is that furthest from the nucleation point, *i.e.*, segments *a*, *b* and *c* correspond to early, middle and later stages of crystal growth respectively. These indicate greater levels of impurities present in **FFA** crystals with greater levels present in crystallizing solutions, as would be expected, and increasing levels of incorporation with increasing growth, in line with the data above.

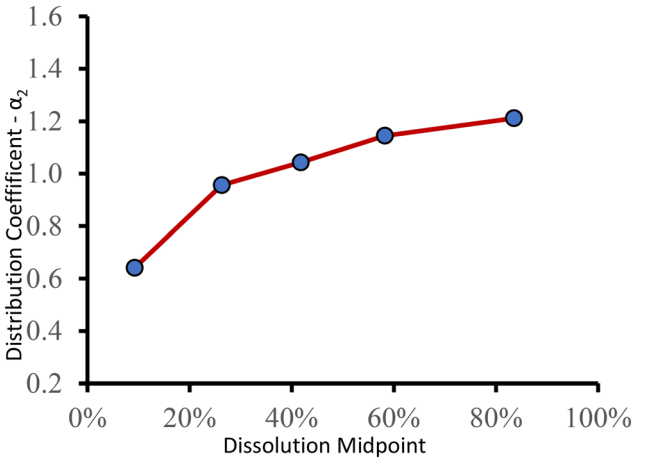


Fig. 14 Plot of α_2 value *vs.* dissolution midpoint of a sample of crystals of **FFA** grown from solution containing 2% molar ratio **H_2FFA**.

The **FFA** analogues examined, **ClFA**, **HF_2FA** and **H_2FFA**, all displayed a good level of incorporation into crystals of **FFA** form III. That behaviour can be rationalized in terms of the reported **FFA** form III crystal structure.[27,35] As noted earlier, there are similarities between the crystal structure of **FFA** form III and **ClFA** form I, for example both contain molecules in similar conformations, and dissimilarities, for example in terms of space groups. Fig. 15 shows the closest distances between atoms in the trifluoromethyl group and atoms on other molecules of **FFA** in the form III crystal structure, visualised using Mercury.[36] The orientation of the trifluoromethyl group is such that two such groups on adjacent molecules are positioned facing each other at a distance of 4.156 Å (C···C) or 3.038 Å (F···F). The only defined intermolecular stabilising interaction is one in which the trifluoromethyl group participates is a 2.590 Å hydrogen bond between one of the fluorines and a neighbouring aromatic C–H proton. It would seem reasonable that the **FFA** form III lattice could facilitate replacement of some trifluoromethyl groups with a sterically smaller group of similar electronegativity. As noted in the Introduction, a chlorine atom would constitute such as group, which would also be supported by the similarities between the **FFA** form III and **ClFA** form I crystal structures. Hence, the extent of

Table 4 Levels, as mol%, of impurities in very elongated needles of **FFA** grown from saturated acetonitrile solutions, in crystal segments *a*, *b* and *c*, in which segment *a* is that closest to the nucleation point, segment *b* is the central segment and segment *c* is that furthers from the nucleation point

Impurity	Mol% impurity level in solution	Mol% impurity in segment		
		a	*b*	*c*
ClFA	4.02	3.44	3.66	3.80
	5.08	4.35	4.69	4.83
HF_2FA	3.46	2.43	2.46	2.52
	5.96	3.93	3.99	4.10
H_2FFA	2.51	1.49	1.54	1.59
	3.32	2.36	2.43	2.51

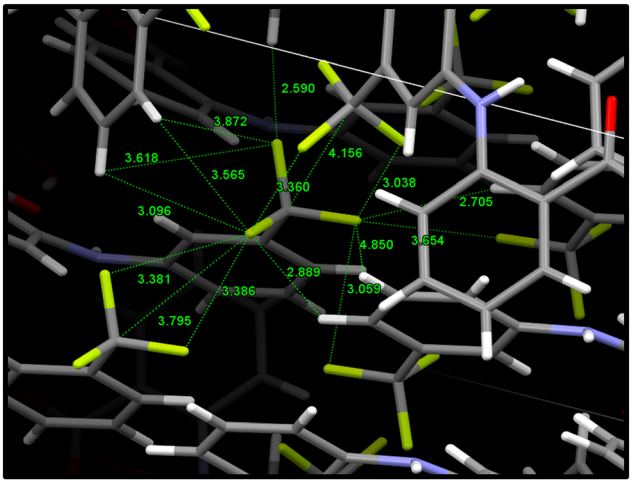


Fig. 15 Closest distances between the trifluoromethyl group of **FFA** and neighbouring atoms in the **FFA** form III crystal structure,[27] visualised by Mercury.[36]

incorporation of **ClFA** is rationalizable. While crystal structures of **HF_2FA** or **H_2FFA** are not available for similar comparisons, the structural similarity between the CF_3, CHF_2 and CH_2F groups would support a similar conclusion in their cases.

The smaller size of the chloro group compared to the trifluoromethyl group, and their similar electronegativities, would facilitate replacement of **FFA** molecules with **ClFA** molecules, consistent with the high degree of incorporation observed. Incorporation of **ClFA** would result in some degree of loss of hydrogen bonding related lattice stabilization, which may be related to the change to a crystal lattice more resembling **ClFA** at **ClFA** levels above *ca.* 25%. As noted above, incorporation of impurities can affect the appearance of the **FFA** form III and form I melting endotherms in DSC analyses, *e.g.*, previous work has shown that the analogue 2-(3-tolylamino)benzoic acid was found to enhance appearance of the **FFA** form III melting endotherm relative to that of form I.[21] By contrast, incorporation of **ClFA** was found to favour enhancement of the form I endotherm, which may be related to loss of form III crystal lattice stability at moderate to high **ClFA** levels. The difluoromethyl and fluoromethyl groups of **HF_2FA** and **H_2FFA** are sterically larger than the chloro group of **ClFA** but are smaller than a trifluoromethyl group and would retain a great degree of the **FFA** form III C–H···F hydrogen bonding. It is reasonable that they would both be well incorporated into the **FFA** form III lattice, as was observed. In DSC analysis, presence of either **HF_2FA** or **H_2FFA** impurity suppressed transformation from **FFA** form III to form I. In that, their behaviour was more similar to that of 2-(3-tolylamino)benzoic acid, as reported,[21] rather than that of **ClFA**.

Conclusions

Occurrence of impurities is a commonplace feature of pharmaceutical process chemistry, for example batches of fluorine-containing drug substance compounds are often found to have some levels of the corresponding desfluoro analogues as impurities. Such impurities are often difficult to adequately remove by crystallization, which is the most important method of product isolation and purification. A basis for such behaviour would be a high degree of incorporation of the impurities into the drug substance crystal lattice, with associated phase behaviour such as solid solution formation. In this work, we have examined the incorporation of such impurities related to the anti-inflammatory compound flufenamic acid, **FFA**, which contains a trifluoromethyl group, the related compounds studied as impurities being the difluoromethyl and fluoromethyl analogues, **HF_2FA** and **H_2FFA**, and the corresponding chloro analogue, **ClFA**, as the chloro group has similar steric and electronic properties to the trifluoromethyl group. This contrasts with previous research which focused on non-polar groups with varying steric demands.[21]

The degree of incorporation of these compounds into crystals of **FFA** was found to vary linearly with the extent of the impurities in the crystallizing solutions with slopes of the lines of *ca.* 0.7 to 1.0, indicating incorporation comparable with that of **FFA** itself. PXRD and DSC studies of crystals containing **FFA** and **ClFA** observed transition from the crystal lattice of **FFA** form III, the **FFA** polymorph obtained in these crystallizations, to that for **ClFA** form I, likewise the form of **ClFA** obtained, with the transition occurring at relatively low proportion of **ClFA**, *e.g. ca.* 25%. The phase behaviour of the **FFA** form III/**ClFA** form I system could be reasonably understood as eutectic with solid solution formation, albeit without clear observation of distinct eutectic and solid solution melting events at low **ClFA** levels. The corresponding binary systems with **FFA** and either **HF_2FA** or **H_2FFA** would likewise be rationalizable as solid solution formation. Partial dissolution studies showed that each of the three impurities studied were present throughout the full crystal growth of the **FFA** crystals, at broadly similar levels, usually with some increase in incorporation at the last stages of crystal growth. This is strong evidence of the systematic inclusion of these impurities during crystal growth and against their inclusion by, for example, surface deposition or absorption, localised inclusion, entrapment by particle agglomeration, or other such mechanisms not involving the actual crystal growth process.

The impurity incorporation results were also considered in term of parameters recommended in the literature for assessing impurity incorporation or rejection in crystallizations. Use of the selectively parameter, α_1, of Urwin *et al.* showed that it would be difficult to remove these impurities by recrystallizations if the impurities were present in solution at the levels studied. Use of the Kitamura and Nakai distribution coefficient, α_2, showed that the degree of discrimination achieved by the crystallization process was not high at any stage of the crystallizations and decreased somewhat in the later stages of crystal growth. As defined,

 This journal is © The Royal Society of Chemistry 2026

both of these parameters are closely related and essentially both indicate that it would be difficult to completely exclude these impurities from **FFA** by crystallization. Examination of the crystal structure of **FFA** form III supports the observation that molecules of **ClFA**, **HF_2FA** or **H_2FFA** could quite reasonably replace some **FFA** molecules, with some loss of lattice stability associated with C–H···F bonding, especially with **ClFA** inclusion, which may be related to the observed switch to the **ClFA** form I crystal lattice in **FFA**/**ClFA** mixtures at relatively low **ClFA** levels.

For a compound such as **FFA**, impurities such as **ClFA**, **HF_2FA** or **H_2FFA** could be viewed as constituting 'worst case scenarios' for purification by crystallization, in that the impurities have good potential to substitute for **FFA** molecules in the **FFA** crystal lattice, leading to poor selectivity and discrimination in the crystallization process, resulting in high degrees of incorporation. The results of the partial dissolution analyses show that this incorporation occurred throughout the process of crystal growth, *i.e.*, was part of the process. Purging of such impurities would therefore require suppressing their occurrence in the crystallization feedstock, *e.g.*, by improving the process chemistry or the quality of the raw materials. The methods described which underpinned these findings could be helpful in cases of impurities proving resistant to purging by crystallization.

Author contributions

T. B., conceptualisation, investigation, writing; R. A. C., conceptualisation, funding acquisition, supervision, writing; H. A. M., conceptualisation, funding acquisition, supervision, writing.

Conflicts of interest

There are no conflicts to declare.

Data availability

Supporting this article have been included as part of the supplementary information (SI).

The above and all other data for this article are available at Cork Open Research Archive (CORA) at https://hdl.handle.net/10468/13652.

Supplementary information: IR, ^{1}H NMR and ^{13}C NMR spectra; HPLC calibration data, PXRDs, morphology images, DSCs, partial dissolution data. See DOI: https://doi.org/10.1039/d6ce00346j.

Acknowledgements

We are grateful to Alkermes Pharma Ireland Ltd and the Irish Research Council, now Research Ireland, for provision of support under grant number EPSPG/2016/179 and to Science Foundation Ireland, now Research Ireland, under grant number SFI 12/RC/2275_P2.

Notes and references

1 H. A. Moynihan and D. E. Horgan, *Org. Process Res. Dev.*, 2017, **21**, 689–704.
2 S. J. Urwin, G. Levilain, I. Marziano, J. M. Merritt, I. Houson and J. H. Ter Horst, *Org. Process Res. Dev.*, 2020, **24**, 1443–1456.
3 Y. Deng, Q. Xie, M. G. LaPoprte, A. T. A. Chasnoff, M. A. Mortensen, D. Patra, S. A. Putrelo, R. S. Antonovich, H. Coa, Y. Yan, A. J. Cooper, S. R. Rippin, M. D. Alexander, P. T. Kumar, M. S. Hendi, Y-. H. Lee, T. Hainmowitz and S. M. Condon, *Org. Process Res. Dev.*, 2016, **20**, 242–252.
4 M. M. Hansen, D. J. Jarmer, E. Arslantas, A. C. DeBaillie, A. L. Frederick, M. Harding, D. W. Hoard, A. Hollister, D. Huber, S. P. Kolis, J. E. Kuenhe-Willmore, T. Kull, M. E. Laurila, R. J. Linder, T. J. Martin, J. R. Martinelli, M. J. McCulley, R. N. Richey, D. R. Starkey, J. A. Ward, N. Zaborenko and T. Zweifel, *Org. Process Res. Dev.*, 2015, **19**, 1214–1230.
5 H. Lorenz and W. Beckmann, Purification by Crystallization, in *Crystallization: Basic Concepts and Industrial Applications*, ed. W. Beckmann, Wiley-VCH GmbH & Co., 2013, ch. 7, pp. 129–148.
6 M. Paolello, S. S. Mohajerani, B. Linehan, F. Ricci, G. Capellades and F. L. Nordstrom, *Cryst. Growth Des.*, 2024, **24**, 2188–2201.
7 P. Prasher and M. Sharma, *Drug Dev. Res.*, 2021, **82**, 945–958.
8 V. López-Mejías, J. W. Kampf and A. J. Matzger, *J. Am. Chem. Soc.*, 2012, **134**, 9872–9875.
9 K. Zhang, N. Fellah, V. López-Mejías and M. D. Ward, *Cryst. Growth Des.*, 2020, **20**, 7098–7103.
10 A. J. Gordon and R. A. Ford, *The Chemist's Companion: A Handbook of Practical Data, Techniques, and References*, Wiley, New York, 1972.
11 P. R. Wells, Group Electronegativities, from *Progress in Physical Organic Chemistry*, ed. A. Streitwieser and R. W. Taft Wiley, New York, 1968.
12 A. Bondi, *J. Phys. Chem.*, 1964, **68**, 441–451.
13 R. Todeschini and V. Consonni, *Handbook of Molecular Descriptors*, Wiley-VCH, 2000.
14 B. E. Smart, *Characteristics of C-F Systems, from Organofluorine Chemistry: Principles and Commerical Applications*, ed. R. E. Banks, B. E. Smart and J. C. Tatlow, Springer Science and Business Media, New York, 1994.
15 X. J. Li and Z. Z. Zeng, *Chem. Res. Chin. Univ.*, 2006, **22**, 6–10.
16 X. Mei, A. T. August and C. Wolf, *J. Org. Chem.*, 2006, **71**, 142–149.
17 V. López-Mejías and A. J. Matzger, *Cryst. Growth Des.*, 2015, **15**, 3955–3962.
18 L. Gorelik, M. Brickelmaier and A. Lugovskoy, Compositions And Methods For The Treatment Of Progressive Multifocal Leukoencephalopathy (PML), US9233107B2, 2016.
19 H. A. Moynihan and D. Armstrong, *CrystEngComm*, 2018, **20**, 2617–2633.
20 H. A. Moynihan and D. Armstrong, *RSC Adv.*, 2019, **9**, 21405–21417.

21 T. Bourke, R. A. Chiarella and H. A. Moynihan, *CrystEngComm*, 2024, **26**, 6837–6843.
22 R. F. Pellón, R. Carrasco, T. Márquez and T. Mamposo, *Tetrahedron Lett.*, 1997, **38**, 5107–5110.
23 J. S. Kaltenbronn, R. A. Scherrer, F. W. Short, E. M. Jones, H. R. Beatty, M. M. Saka, C. V. Winder, J. Wax and W. R. N. Williamson, *Arzneim. Forsch.*, 1983, **14**, 621–627.
24 J. F. McConnell, *Cryst. Struct. Commun.*, 1973, **3**, 459–461.
25 H. M. Krishna Murthy, T. N. Bhat and M. Vijayan, *Acta Crystallogr., Sect. B*, 1982, **38**, 315–317.
26 E. H. Lee and S. R. Byrn, *J. Pharm. Sci.*, 2010, **99**, 4013–4022.
27 S. P. Delaney, T. M. Smith and T. M. Korter, *J. Mol. Struct.*, 2014, **1078**, 83–89.
28 S. Romero, P. Bustamante, B. Escalera, M. Cirri and P. Mura, *J. Therm. Anal. Calorim.*, 2004, **77**, 541–554.
29 J. Krc, *Microscope*, 1977, **25**, 31–45.
30 H. Yuerong, H. Wikström, S. R. Byrn and L. S. Taylor, *J. Pharm. Biomed. Anal.*, 2007, **45**, 546–551.
31 A. Burger and R. Ramberger, *Microchim. Acta*, 1980, **73**, 17–28.
32 S. Black, L. Dang, C. Liu and H. Wei, *Org. Process Res. Dev.*, 2013, **17**, 486–492.
33 F. L. Nordstrom and F. Ricci, *Cryst. Growth Des.*, 2026, **26**, 446–466.
34 M. Kitamura and T. Nakai, *J. Chem. Eng. Jpn.*, 1983, **16**, 288–293.
35 C. R. Groom, I. J. Bruno, M. P. Lightfoot and S. C. Ward, *Acta Crystallogr., Sect. B: Struct. Sci., Cryst. Eng. Mater.*, 2016, **72**, 171–179.
36 C. F. Macrae, I. J. Bruno, J. A. Chisholm, P. R. Edgington, P. McCabe, E. Pidcock, L. Rodriguez-Monge, R. Taylor, J. van de Streek and P. A. Wood, *J. Appl. Crystallogr.*, 2008, **41**, 466–470.

 This journal is © The Royal Society of Chemistry 2026